Two Series of Solvent-Dependent Lanthanide Coordination Polymers Demonstrating Tunable Luminescence and Catalysis Properties

Na Wei,[†] Ming-Yang Zhang,[†] Xiao-Nan Zhang,[†] Guang-Ming Li,[‡] Xiang-Dong Zhang,[†] and Zheng-Bo Han*[,†]

[†]College of Chemistry, Liaoning University, Shenyang 110036, P. R. China
[‡]College of Chemistry and Material Science, Heilongjiang University, Harbin 150080, P. R. China

Ⓢ *Supporting Information*

ABSTRACT: Two series of lanthanide−organic frameworks with the formulas $[Ln(BTATB)(DMF)_2(H_2O)]·DMF·2H_2O$ (Ln = La (**1a**), Eu (**2a**), Tb (**3a**), Er (**4a**)) and $[Ln(BTATB)(H_2O)_2]·2DMA·4H_2O$ (Ln = Er (**1b**), Yb (**2b**), Lu (**3b**)), respectively, were solvothermally synthesized from 4,4′,4″-(benzene-1,3,5-triyltris(azanediyl))tribenzoate (H_3BTATB) and $Ln(NO_3)_3$ under DMF or DMA media and characterized by thermogravimetric analyses, IR spectroscopy, X-ray powder diffraction, and single crystal X-ray diffraction. X-ray single-crystal diffraction analyses for these complexes revealed that

series A features an interesting 2D interdigitated layer architecture with (6,3) topology. Series B exhibits a 2D bilayer structure. The luminescence properties were studied, and the results showed that complex **3a** displayed strong fluorescent emission in the visible region, where the emission intensities of **3a** are enhanced upon the addition of Zn^{2+}, demonstrating Zn^{2+}-modulated fluorescence. Yb(III) complex **2b** emits typical near-infrared luminescence (983 nm) in DMF (λ_{ex} = 315 nm). The Knoevenagel condensation reaction (benzaldehyde and malononitrile or ethyl cyanoacetate in acetonitrile) was studied using **3a** and **2b** as catalysts. The results showed that the conversion rates of reactions catalyzed by **3a** increased to 99 and 42%, respectively, whereas the reactions catalyzed by **2b** exhibited lower conversion rates.
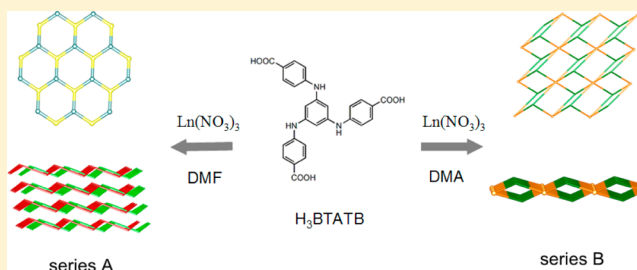
INTRODUCTION

For decades, the design and synthesis of novel lanthanide−organic frameworks (LnOFs) has been a field of rapid growth in supramolecular and materials chemistry because of their exceptionally artistic architectures and potential applications, such as gas adsorption and separation, heterogeneous catalysis, and luminescence.[1] LnOFs offer high photoluminescence efficiencies, unique line-like emission bands, substantial Stokes shifts, and long luminescence lifetimes.[2] It should be noted that the unique luminescence properties of lanthanide complexes result from f−f transitions generated via the "antenna effect",[3] which have made them one of the essential components in the preparation of advanced materials.[4] Recently, studies on luminescent LnOFs for sensing metal ions have resulted in their significant development, and some successful fluorescent probes have been employed to determine the concentration of metal ions, such as Zn^{2+}, Cu^{2+}, and Fe^{3+}.[5]

The use of MOFs as catalysts is another hot topic in this field in addition to their use as luminescent probes. The catalytic activity of MOF materials results from the metal center in the structure or the catalytically active functional organic sites on the organic ligand, such as noncoordinated amino groups.[6] Detailed studies on the catalytic performance of MOFs with catalysis taking place at the metal center have been reported recently.[7] However, only a few proof-of-concept studies of MOFs with catalysis taking place at the organic ligand have been reported.[8]

These excellent properties and extensive applications are mostly attributed to the distinct structure and composition of this material. It is well-known that during the self-assembly process the experimental conditions play a significant role in the growth of the crystals, such as the reaction temperature, reaction period, concentrations of the raw materials, and so on.[9] Among these factors, solvent molecules as guests sometimes behave like structure-directing agents during the self-assembly process and generate new structures in different solvents.[10]

Herein, we prepared a new tripodal carboxylate ligand with functional groups, namely, H_3BTATB (BTATB = 4,4′,4″-(benzene-1,3,5-triyltris(azanediyl))tribenzoate). The tripodal ligand was chosen for the following reasons: (i) a ligand with longer arms may facilitate the formation of novel unusual network topologies; (ii) the lanthanide ion is a hard acid and prefers oxygen to nitrogen donors, so the available amino functional groups on the ligand may coordinate with other metal ions after the MOFs are constructed, a characteristic that may alter their fluorescence; and (iii) the amino groups on the ligand may impart the material with catalytic activity. As the result of this rational design, we herein present two series of lanthanide coordination polymers, $[Ln(BTATB)(DMF)_2(H_2O)]·DMF·$

Table 1. Crystallographic Data for Series A

	1a	2a	3a	4a
empirical formula	$C_{36}H_{45}LaN_6O_{12}$	$C_{36}H_{45}EuN_6O_{12}$	$C_{36}H_{45}TbN_6O_{12}$	$C_{36}H_{45}ErN_6O_{12}$
formula weight	892.68	905.74	912.71	921.04
wavelength (Å)	0.710 73	0.710 73	0.710 73	1.541 78
crystal system	monoclinic	monoclinic	monoclinic	monoclinic
space group	$P\bar{1}$	$P\bar{1}$	$P\bar{1}$	$P\bar{1}$
a (Å)	10.071(4)	9.9905 (5)	9.9808(5)	10.0286(3)
b (Å)	13.401(6)	13.2420(6)	13.2130(7)	13.2632(3)
c (Å)	15.645(7)	15.4464(7)	15.4078(8)	15.4066(5)
α (deg)	106.901(7)	107.2920(10)	107.4350(10)	107.730(3)
β (deg)	96.009(7)	95.8580(10)	95.8690(10)	96.065(2)
γ (deg)	96.899(7)	97.4250(10)	97.2850(10)	96.308(2)
V (Å³)	1983.8(15)	1913.33(16)	1901.69(17)	1919.04(10)
Z	2	2	2	2
D_c (mg m⁻³)	1.491	1.572	1.594	1.594
μ (mm⁻¹)	1.144	1.709	1.930	4.654
$F(000)$	908	924	928	934
range for data collection (deg)	1.61−26.00	1.40−26.00	1.40−26.00	3.04−72.18
reflections collected	10 794	10 630	10 599	13 429
max, min transmission	0.7583, 0.6848	0.6905, 0.5798	0.5763, 0.4943	0.4303, 0.2866
T (K)	293(2)	293(2)	293(2)	293(2)
data/restraints/parameters	7632/0/451	7416/0/451	7379/0/452	7383/0/497
final R indices $[I > 2\sigma(I)]^a$	$R_1 = 0.0521$, $wR_2 = 0.1189$	$R_1 = 0.0438$, $wR_2 = 0.1097$	$R_1 = 0.0446$, $wR_2 = 0.0970$	$R_1 = 0.0400$, $wR_2 = 0.1082$
R indices (all data)	$R_1 = 0.0674$, $wR_2 = 0.1272$	$R_1 = 0.0554$, $wR_2 = 0.1155$	$R_1 = 0.0580$, $wR_2 = 0.1024$	$R_1 = 0.0426$, $wR_2 = 0.1118$
largest diff. peak and hole (e Å⁻³)	1.045, −1.170	1.133, −0.903	0.801, −0.864	1.835, −0.969

$^a R_1 = \sum ||F_o| - |F_c||/\sum |F_o|$; $wR_2 = \sum[w(F_o{}^2 - F_c{}^2)^2]/\sum[w(F_o{}^2)^2]^{1/2}$

$2H_2O$ (series A; Ln = La (**1a**), Eu (**2a**), Tb (**3a**), Er (**4a**)) and $[Ln(BTATB)(H_2O)_2]·2DMA·4H_2O$ (series B; Ln = Er (**1b**), Yb (**2b**), Lu (**3b**)), that were generated by changing only the reaction solvent. More interestingly, the emission intensity of **3a** could be modulated by Zn^{2+} among other metal ions. **3a** and **2b** also show catalytic activity toward Knoevenagel condensation reactions.

■ EXPERIMENTAL SECTION

Materials and Methods. All chemicals used for synthesis were commercially available reagents of analytical grade and were used without further purification. C, H, and N microanalyses were carried out with a PerkinElmer 240 elemental analyzer. The FT-IR spectra were recorded from KBr pellets in the 4000−400 cm⁻¹ range on a Nicolet 5DX spectrometer. Thermogravimetric analyses (TGA) were recorded on a PerkinElmer Pyris 1 (25−600 °C, 5 °C min⁻¹, flowing $N_2(g)$). X-ray powder diffraction (PXRD) patterns were recorded with a Bruker AXS D8 advanced automated diffractometer with Cu Kα radiation. Luminescence spectra for the solid and liquid samples were investigated with a Hitachi F-4500 fluorescence spectrophotometer and Varian Cary Eclipse Fluorescence spectrophotometer, respectively. The products of catalysis reactions were monitored by gas chromatography with a SP-2100A gas chromatograph.

Synthesis of Triethyl 4,4′,4″-(Benzene-1,3,5-triyltris(azanediyl))-tribenzoate, 1. Concentrated hydrochloric acid (5.2 mL), phloroglucinol (12.6 g, 0.10 mol), 4-aminobenzoic acid ethyl ester (66.0 g, 0.40 mol), and diethylene glycol dimethyl ether (45 mL) were added to a 100 mL round-bottomed flask, and the mixture was stirred at 130 °C for 7 h. Yellow crystals appeared as the suspension cooled. The crystals were washed with diethylene glycol dimethyl ether and dried in an oven to yield 35.2 g of **1** (35.2 g, 70%). ¹H NMR (DMSO-d_6): δ 1.30 (t, 9H), 4.26 (q, 6H), 6.62 (s, 3H), 7.13 (d, 6H), 8.38 (d, 6H), 8.78 (s, 3H).

Synthesis of H_3BTATB, 4,4′,4″-(Benzene-1,3,5-triyltris(azanediyl))-tribenzoic acid, 2. Compound **1** (10.0 g, 0.019 mol) was suspended in 150.0 mL of THF/MeOH (v/v 1:1) followed by the addition of 60.0 mL of a 10% NaOH solution. The mixture was stirred overnight. The pH was adjusted to approximately 3 using hydrochloric acid. The resulting brown precipitate was collected by centrifugation, washed with water, and dried under vacuum to yield **2** (8.0 g, 90%). ¹H NMR (DMSO-d_6): δ 6.62 (s, 3H), 7.13 (d, 6H), 7.82 (d, 6H), 8.73 (s, 3H).

*Preparation of $[Ln(BTATB)(DMF)_2(H_2O)]·DMF·2H_2O$ (Series A; Ln = La (**1a**), Eu (**2a**), Tb (**3a**), Er (**4a**)).* Complexes **1a**−**4a** were synthesized by the following procedure: $Ln(NO_3)_3·6H_2O$ (30 mg) was added to a DMF/H_2O (1:1, 3 mL) solution of H_3BTATB (15 mg), and the mixture was stirred for ca. 20 min in air. It was then heated at 105 °C for 2 days to produce brown block crystals.

*$[La(BTATB)(DMF)_2(H_2O)]·DMF·2H_2O$ (**1a**).* Yield: ca. 68%. Anal. calcd (%) for **1a** $C_{36}H_{45}LaN_6O_{12}$ (%): C, 48.44; H, 5.08; N, 9.41. Found: C, 48.54; H, 5.11; N, 9.38. IR (KBr, cm⁻¹): 3448 (s), 1654 (s), 1586 (s), 1517 (m), 1392 (vs), 1322 (w), 1261 (w), 1168 (w), 844 (w), 787 (w).

*$[Eu(BTATB)(DMF)_2(H_2O)]·DMF·2H_2O$ (**2a**).* Yield: ca. 70%. Anal. calcd (%) for **2a** $C_{36}H_{45}EuN_6O_{12}$ (%): C, 47.74; H, 5.01; N, 9.28. Found: C, 47.54; H, 5.21; N, 9.01. IR (KBr, cm⁻¹): 3420 (s), 2925 (w), 1654 (s), 1586 (s), 1519 (m), 1396 (vs), 1322 (m), 1261 (w), 1167 (w), 1135 (w), 1101 (w), 844 (w), 786 (m).

*$[Tb(BTATB)(DMF)_2(H_2O)]·DMF·2H_2O$ (**3a**).* Yield: ca. 71%. Anal. calcd (%) for **3a** $C_{36}H_{45}TbN_6O_{12}$ (%): C, 47.37; H, 4.97; N, 9.21. Found: C, 47.21; H, 5.07; N, 9.03. IR (KBr, cm⁻¹): 3425 (s), 2924 (w), 1655 (s), 1586 (s), 1520 (m), 1398 (vs), 1321 (m), 1260 (w), 1166 (w), 1135 (w), 1101 (w), 843 (w), 786 (m).

*$[Er(BTATB)(DMF)_2(H_2O)]·DMF·2H_2O$ (**4a**).* Yield: ca. 30%. Anal. calcd (%) for **4a** $C_{36}H_{45}ErN_6O_{12}$ (%): C, 46.95; H, 4.92; N, 9.12. Found: C, 46.71; H, 5.01; N, 9.07. IR (KBr, cm⁻¹): 3428 (s), 2927 (w), 1652 (s), 1587 (s), 1521 (m), 1402 (vs), 1325 (m), 1258 (w), 1164 (w), 1137 (w), 1105 (w), 845 (w), 789 (m).

*Preparation of $[Ln(BTATB)(H_2O)_2]·2DMA·4H_2O$ (Series B; Ln = Er (**1b**), Yb (**2b**), Lu(**3b**)).* Complexes **1b**−**3b** were synthesized by the following procedure: $Ln(NO_3)_3·6H_2O$ (30 mg) was added to a DMA/H_2O (1:1, 3 mL) solution of H_3BTATB (15 mg), and the mixture was stirred for ca. 20 min in air. It was then heated at 105 °C for 2 days to produce brown block crystals.

*$[Er(BTATB)(H_2O)_2]·2DMA·4H_2O$ (**1b**).* Yield: ca. 72%. Anal. calcd (%) for **1b** $C_{35}H_{48}ErN_5O_{14}$ (%): C, 45.20; H, 5.20; N, 7.53. Found: C, 45.32; H, 5.24; N, 7.47. IR (KBr, cm⁻¹): 3399 (s), 2922 (w), 1592 (s), 1518 (m), 1412 (vs), 1318 (m), 1256 (m), 1174 (m), 839 (w), 786 (m).

[Yb(BTATB)(H₂O)₂]·2DMA·4H₂O (2b). Yield: ca. 69%. Anal. calcd (%) for **2b** $C_{35}H_{48}YbN_5O_{14}$ (%): C, 44.92; H, 5.17; N, 7.48. Found: C, 44.86; H, 5.21; N,7.62. IR (KBr, cm⁻¹): 3400 (s), 2922 (w), 1593 (s), 1521 (m), 1413 (vs), 1320 (m), 1256 (w), 1174 (w), 786 (m).

[Lu(BTATB)(H₂O)₂]·2DMA·4H₂O (3b). Yield: ca. 67%. Anal. calcd (%) for **3b** $C_{35}H_{48}LuN_5O_{14}$ (%): C, 44.83; H, 5.16; N, 7.47. Found: C, 44.78; H, 5.23; N, 7.51. IR (KBr, cm⁻¹): 3400 (s), 2921 (w), 1593 (s), 1521 (m), 1415 (vs), 1317 (w), 1255 (w), 1174 (w), 836 (w), 786 (m).

X-ray Crystallography. Crystallographic data of all the complexes were collected at 173 K with a Apex II diffractometer with Mo Kα radiation or Cu Kα radiation (λ = 0.71073 or 1.5418 Å) and a graphite monochromator using the ω scan mode. The structure was solved by direct methods and refined on F^2 by full-matrix least-squares using SHELXTL.[11] Crystallographic data and experimental details for structural analyses are summarized in Tables 1 and 2. The CCDC

Table 2. Crystallographic Data for Series B

	1b	2b	3b
empirical formula	$C_{35}H_{48}ErN_5O_{14}$	$C_{35}H_{48}YbN_5O_{14}$	$C_{35}H_{48}LuN_5O_{14}$
formula weight	930.04	935.82	937.75
wavelength (Å)	0.710 73	0.710 73	0.710 73
crystal system	monoclinic	monoclinic	monoclinic
space group	$P\bar{1}$	$P\bar{1}$	$P\bar{1}$
a (Å)	11.8978(4)	11.8938(4)	11.8842(3)
b (Å)	12.4423(4)	12.4541(3)	12.4550(3)
c (Å)	13.2083(5)	13.1622(3)	13.1712(3)
α (deg)	84.049(3)	84.035(2)	83.924(2)
β (deg)	85.054(3)	85.080(2)	84.970(2)
γ (deg)	85.456(3)	85.246(2)	85.196(2)
V (Å³)	1932.65(12)	1926.58(9)	1925.69(8)
Z	2	2	2
D_c (mg m⁻³)	1.433	1.447	1.617
μ (mm⁻¹)	2.232	2.488	2.637
F(000)	840	844	952
range for data collection (deg)	2.93−26.00	2.91−26.00	2.91−26.00
reflections collected	13 979	13 112	15 877
max, min transmission	0.538, 10.4939	0.5023, 0.4612	0.5985, 0.3983
T (K)	293(2)	293(2)	293(2)
data/restraints/parameters	7585/0/437	7576/0/352	7569/0/496
final R indices $[I > 2\sigma(I)]^a$	$R_1 = 0.0590$, $wR_2 = 0.1420$	$R_1 = 0.0272$, $wR_2 = 0.0683$	$R_1 = 0.0374$, $wR_2 = 0.0960$
R indices (all data)	$R_1 = 0.0687$, $wR_2 = 0.1464$	$R_1 = 0.0310$, $wR_2 = 0.0700$	$R_1 = 0.0426$, $wR_2 = 0.0988$
largest diff. peak and hole (e Å⁻³)	4.975, −5.681	0.763, −0.772	2.544, −1.045

$^aR_1 = \sum \|F_o| - |F_c\|/\sum|F_o|;$ $wR_2 = \sum[w(F_o^2 - F_c^2)^2]/\sum[w(F_o^2)^2]^{1/2}$

reference numbers are 988282−988285 for **1a−4a** and 988286−988288 for **1b−3b**. A copy of the data can be obtained free of charge upon request from the CCDC, 12 Union Road, Cambridge CB2 1EZ, UK (Fax: +44(1223)336-033; E-mail: deposit@ccdc.cam.ac.uk).

■ **RESULTS AND DISCUSSION**

The crystals [Ln(BTATB)(DMF)₂(H₂O)]·DMF·2H₂O (Ln = La (**1a**), Eu (**2a**), Tb (**3a**), Er (**4a**)) and [Ln(BTATB)(H₂O)₂]· 2DMA·4H₂O (Ln = Er (**1b**), Yb (**2b**), Lu (**3b**)) are two series of isomorphous coordination frameworks, so **4a** and **1b** are employed as representative examples that will be described in detail.

Single-crystal X-ray diffraction analysis revealed that **4a** crystallizes in the triclinic $P\bar{1}$ space group. **4a** is an interdigitated metal−organic framework; the asymmetric unit of **4a** contains one crystallographically independent Er(III) center, one BTATB ligand, two coordinated DMF molecules, one aqua ligand, one free DMF molecule, and two lattice water molecules. As shown in Figure 1a, each Er(III) center is nine-coordinate and surrounded by six carboxylate oxygen atoms from three individual BTATB ligands, three oxygen atoms from two coordinated DMF molecules, and one aqua ligand, respectively, forming a tricapped trigonal-pyramidal geometry. The BTATB ligand adopts a tri(chelate) coordination mode, and its carboxylate groups are deprotonated.

The Er(III) centers are connected by BTATB ligands to form a 2D wave-like layer with a (6,3) topological net (Figure 1b). A very significant structural feature of **4a** is that two adjacent layers are interdigitated together with the metal ion parts protruding out of the other layer (Figure 1b,c). The aromatic ring distance between two stacked BTATB ligands and a pair of interdigitated layers is 4.11(1) Å, as shown in Figure 1c, and the structure can be defined as stable MOFs with a framework that is interdigitated through π−π stacking. The lanthanide(III) ions usually have a high coordination number because of their large atomic radius, and they tend to form highly connected complex structures. Therefore, it is difficult to produce low-connected structures like a (6,3) net. Although rare-earth coordination polymers with a (6,3) net have been previously reported, Mak et al. reported a coordination polymer {[Er(NO₃)₃(L)₁.₅]·H₂O} (L = 1,2-bis(4-pyridyl)ethane-*N,N′*-dioxide) showing a mat-like composite layer with a (6,3) net,[12] and Jin et al. reported three compounds showing a 2D layer of a (6,3) net.[13] Lanthanide coordination polymers based on oxalate that have a (6,3) net have also been reported.[14] To the best of our knowledge, the LnOF with a (6,3) net stacked in an interdigitated fashion is unprecedented.[15] Furthermore, adjacent interdigitated layers are linked by hydrogen bonds to form a 3D supramolecular framework (Figure 1d).

Single-crystal X-ray diffraction analysis revealed that **1b** crystallizes in the triclinic $P\bar{1}$ space group, which features a 2D bilayer structrue. The asymmetric unit of **1b** is composed of one crystallographically independent Er(III) center, one BTATB ligand, two aqua ligands, two free DMA molecules, and four lattice water molecules. As shown in Figure 2a, each Er(III) center is eight-coordinate and surrounded by eight oxygen atoms, six from the carboxylate atoms of six individual BTATB ligands via two chelating and one syn−anti O,O′-bridge coordination modes; the remaining coordination sites are occupied by two individual aqua ligands. The coordination geometry around the Er(III) center can be described as a distorted dodecahedron, with the O−Er−O bond angles ranging from 54.3(1) to 134.8(1) and the Er−O bond lengths ranging from 2.209(3) to 2.462(3) Å. There is a unique crystallographically independent BTATB ligand in **2b**, of which two carboxylate groups bridge two Er(III) centers in chelating coordination modes, whereas the third carboxylate group bridges two Er(III) centers in a syn−anti O,O′-bridge coordination mode; all of the carboxylate groups of the BTATB ligands are deprotonated. Two near Er(III) centers are bridged by two carboxylate oxygen atoms of carboxylate groups in syn−syn fashion to form a Er(III)···Er(III) dimer (Figure 2b). The Er···Er distance and Er−O−Er bond angles in the dimer are 4.5387(3) Å and 123.6(4)°, respectively. Four Er(III)···Er(III) dimers are further linked by two BTATB ligands to form a 2D bilayer
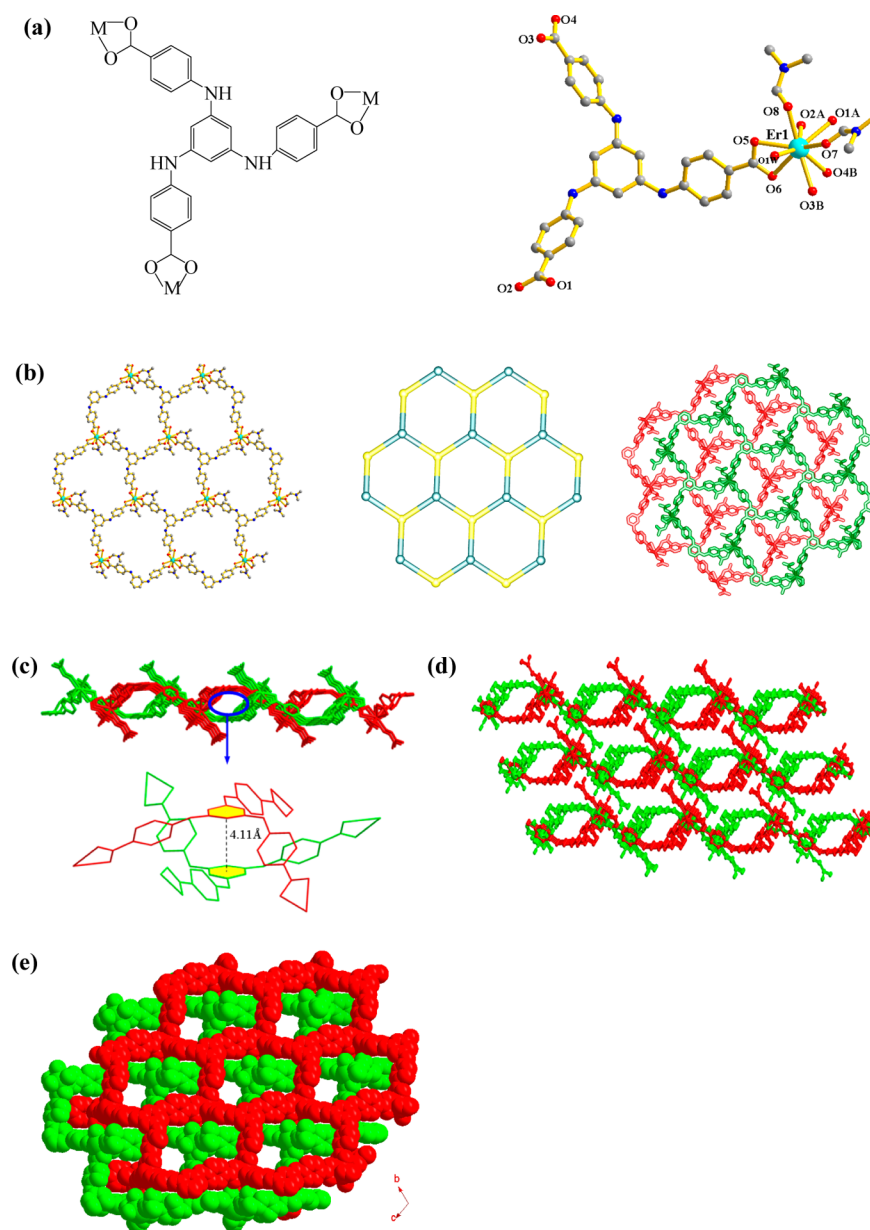
Figure 1. (a) Coordination environment of the Er(III) center in **4a**. Symmetry mode for series A: $x + 1, y - 1, z$. Symmetry mode for series B: $x + 1, y, z + 1$. (b) (6,3) layer of **4a**. (c) Top: side view of 2D interdigitated layer architecture of **4a**. Bottom: distance between two BTATB ligands. (d) Three-dimensional stacking plot of **4a**. (e) Space-filling representation of the 3D structure of **4a** along the a-axis direction (DMF molecules omitted).

structure (Figure 2c,d). Interestingly, the 2D bilayer can be rationalized as a noninterpenetrating CdI$_2$-type network by simplifying the BTATB ligand as a three-connected node (vertex symbol 4^3) and the Er···Er dimer as a six-connected node (vertex symbol 4^{6}6^{6}8^3) (Figure 2e). The CdI$_2$-type network, which can be represented by Wells notation {4$_6^3$}, is one of the Catalan nets known in inorganic compounds such as metal alkoxides and hydroxides.[16] The main topological character of the CdI2 net is that it can be regarded as forming by the offset overlap of two (6,3) nets, but, in fact, it contains only congruent quadrangles similar to those of the (4,4) net.[17] Although coordination networks with a bilayer network have been reported previously, Hill et al. reported four lanthanide(III) coordination polymers with 2D bilayer networks,[18] in which three structures have six-connected topology and a single example has five-connecting topology, and Wang et al. reported four Zn(II) coordination polymers that exhibit different bilayer architectures.[19] To the

best of our knowledge, the 2D lanthanide(III) bilayer coordination polymer with the CdI$_2$-type network is unprecedented. Furthermore, adjacent bilayers are linked by hydrogen bonding to form a 3D supramolecular framework (Figure 2c).

It should be noted that just by changing the solvent under the same reaction conditions several different compounds were synthesized with the same ligand and lanthanide ions. **1b** was synthesized in a similar procedure as that of **4a**, the difference being that DMA was used as the solvent instead of DMF. However, the two complexes display distinct structures. Because different solvents in the solvothermal conditions can lead to a pH change of the reaction system, the reaction microenvironment and the coordination modes of the BTATB ligand change and, consequently, different structures are generated.

Thermal Stability. The simulated and experimental XRD patterns of two series of compounds are shown in Figures S1 and S2, Supporting Information. Their peak positions are almost in
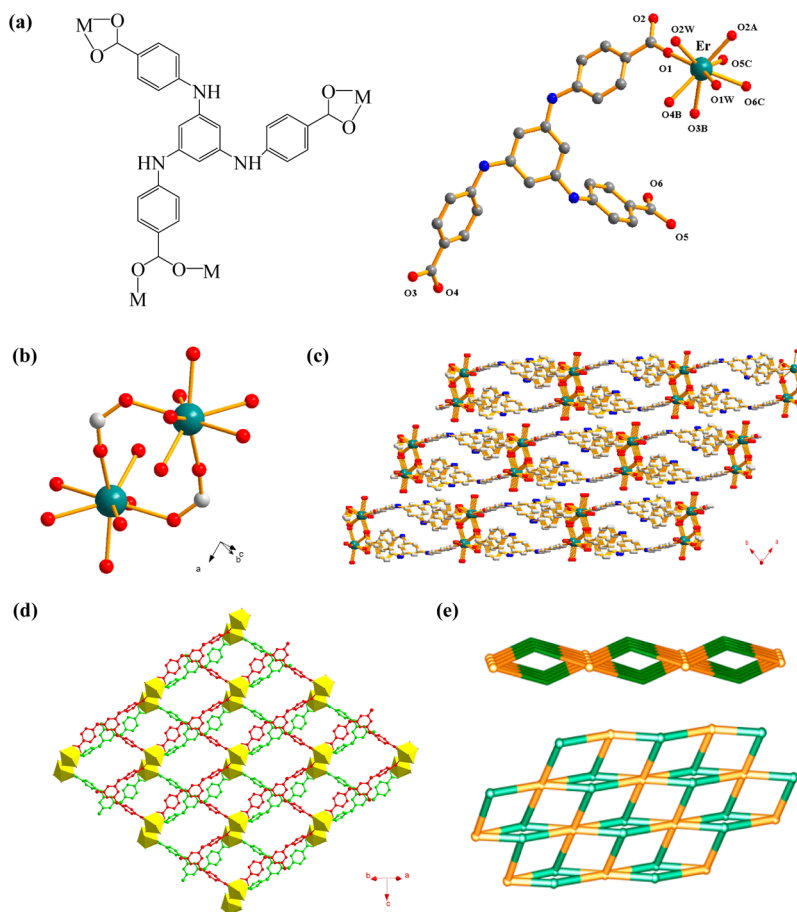
Figure 2. (a) Coordination modes of the BTATB ligand and coordination environment of the Er center in **1b**. Symmetry mode of series A: $1 - x, 2 - y, 1 - z$. Symmetry mode of series B: $2 - x, 1 - y, -z$. C: $1 - x, 2 - y, -z$. (b) Er(III)···Er(III) dimer. (c) and (d) 2D bilayer structure of **1b** (yellow polyhedrons represent the Er dimer). (e) View of the simplified network of **1b**.

agreement with each other, indicating the phase purity of the products. The TGA curve (Figure S3, Supporting Information) of series A shows the first weight loss of 3.1% at ca. 100 °C, which corresponds to the loss of two lattice water molecules (calculated 3.94%). A weight loss of 26.9% occurs between 100 and 400 °C, which corresponds to the loss of one guest DMF, one coordinated water, and two coordinated DMF molecules (calculated 27.9%). The residue was Ln_2O_3 (experimental, 41.2%; calculated, 40.7%). The TGA curve (Figure S4, Supporting Information) of series B demonstrates that the weight loss of the free and coordinated solvent molecules was well-resolved. From 30 to ca. 235 °C, the first weight loss is 18.72%, which corresponds to the weight of two free DMA molecules (calculated 18.62%). The weight loss of 7.6% between 235 and 444 °C may be attributed to the loss of four lattice water molecules (calculated 7.7%) and then decomposition of the complexes upon further heating.

Photoluminescence Properties. Studies on luminescent lanthanides have concentrated on Sm(III), Eu(III), Tb(III), and Dy(III) ions in the visible region, so the luminescence properties of **3a** were investigated. The emission spectrum of **3a** was collected in the range 380−700 nm in a methanol suspension and in the solid state (Figure S5, Supporting Information) at room temperature under excitation at 360 nm, and it exhibits the characteristic transition of the Tb^{3+} ion:[20] $^5D_4 \rightarrow {}^7F_J$ ($J = 3, 4, 5, 6$), namely, $^5D_4 \rightarrow {}^7F_6$ (491 nm), $^5D_4 \rightarrow {}^7F_5$ (546 nm), $^5D_4 \rightarrow {}^7F_4$ (586 nm), and $^5D_4 \rightarrow {}^7F_3$ (622 nm). Among these

transitions, $^5D_4 \rightarrow {}^7F_5$ (546 nm) is the strongest. The effects of a variety of biologically relevant cations, Co^{2+}, Cu^{2+}, Cd^{2+}, Pb^{2+}, Hg^{2+}, and Zn^{2+}, on the fluorescent intensity of **3a** were investigated, and the result indicates that the emission intensity of **3a** increased significantly upon addition of Zn^{2+}. More remarkably, the emission intensity of **3a** increased gradually upon addition of 1−3 equiv of Zn^{2+} with respect to **3a** (Figure 3a). The highest peak at 577 nm is at least twice as intense as the corresponding band in the solution without Zn^{2+}. The introduction of other metal ions caused the intensity either to be unchanged or weakened (Figure 3b).

It is well-known that the luminescent intensity of Ln^{3+} relies on the efficiency of the energy transfer from the ligand to the Ln^{3+} center.[20a] Chen et al. prepared $[Eu(pdc)_{1.5}(DMF)]$ with Lewis basic pyridyl sites for sensing Cu^{2+} and Co^{2+},[5d] and Liu et al. reported Ag^+-modulated luminescence for a Eu(III) complex;[5c] in this case, the luminescent intensity was enhanced because Ag^+ is coordinated by the azacyclic amine group from the tetra(amino acid) ligand. As with the study of the reported metal-sensitive luminescent lanthanide probes, the enhancement of the luminescent intensity in our investigation may result from Zn^{2+} aggrandizing the antenna efficiency of the BTATB organic linkers, diminishing the f−f transitions of Tb^{3+} and leading to more effective intramolecular energy transfer from the BTATB ligand to Ln^{3+} with the addition of Zn^{2+}. The luminescence properties of **1a** were also measured, but no emissions were observed.
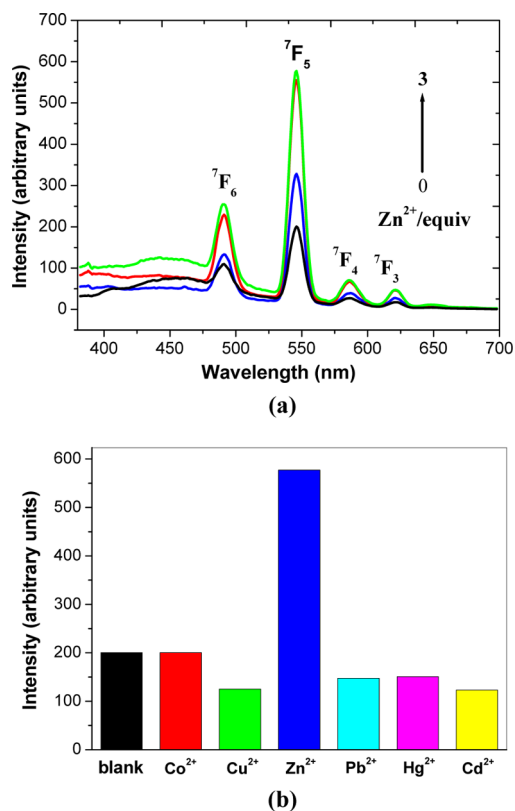
Figure 3. (a) Emission spectra of complex **3a** in methanol at room temperature in the presence of 0−3 equiv of Zn^{2+} ions with respect to **3a**: black, no addition; blue, 1 equiv; red, 2 equiv; green, 3 equiv. **3a** was excited at 360 nm. (b) Room-temperature luminescent intensity of **3a** at 546 nm in a methanol suspension upon addition of various metal ions (excited at 360 nm).

Recently, many scientists have begun to exploit developments in the detection of near-infrared luminescence to study the luminescence from Nd(III), Er(III), and Yb(III) complexes,[21] so the near-infrared emission of **2b** was measured. When complex **2b** was excited at 315 nm in a DMF solution, it led to a typical metal-centered near-infrared luminescence at 983 nm (Figure 4). Yb(III) is a special case among the near-infrared-emitting lanthanide ions because the Yb(III) ion has only one excited 4f
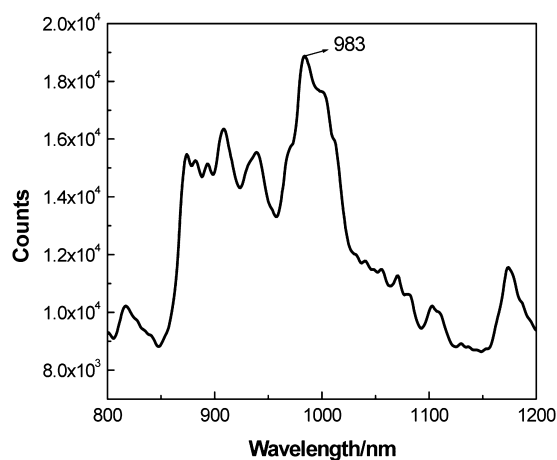
Figure 4. Near-infrared emission spectrum of **2b** in DMF upon excitation at 315 nm.

level, namely, the $^2F_{5/2}$ level, so its luminescence observed at ca. 980 nm is assigned to the $^2F_{5/2} \rightarrow {}^2F_{7/2}$ transition.[22]

Catalysis Properties. The amino-based metal−organic frameworks are stable, solid, basic catalysts in the Knoevenagel condensation reaction, and their structural features endow the MOFs with size- or shape-selective catalysis.[23] In order to investigate the size-selective catalysis of the two series of complexes, we took a systematic approach by varying the size and shape of the substrate. The Knoevenagel condensation reaction of benzaldehyde with each of the active methylene compounds (malononitrile and ethyl cyanoacetate) was performed with catalysis by **3a** and **2b** as representative examples.

A solution of equivalent amounts of benzaldehyde (0.87 nm × 0.61 nm) and malononitrile (0.69 nm × 0.45 nm) or ethyl cyanoacetate (1.03 nm × 0.45 nm) was mixed in acetonitrile. This solution was added at 60 °C to a suspension of **3a** or **2b** in acetonitrile (Scheme 1), and the progress of the reaction was

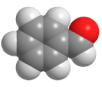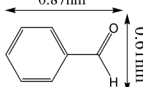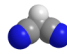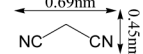**Scheme 1. Knoevenagel Condensation Reaction Catalyzed by 3a and 2b**
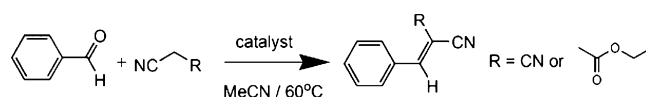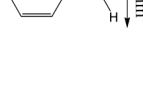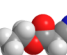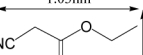

monitored using gas chromatography (see the Supporting Information). As shown in Table 3, benzaldehyde (size, 0.87 nm × 0.61 nm; shape, linear) and malononitrile (0.69 nm × 0.45 nm) lead to a 99% conversion when the reaction is catalyzed by **3a**. In the case of ethyl cyanoacetate (1.03 × 0.45 nm), **3a** resulted in a 42% conversion. The conversion of the reactions catalyzed by **2b** is 33 and 3%, respectively, which is lower than that of reactions catalyzed by **3a**.

The distinct conversion rates reflect the size and shape selectivity of the catalyst. **3a** may lose coordinated DMF molecules during the reaction, obtaining 1D microporous channels (0.75 × 0.64 nm) in the structure (Figure 1e) in which these catalytic reactions probably take place. If the reactions were catalyzed only on the external surface of the MOF crystals, then the difference in the conversion rates between the two reaction systems would be small. Moreover, as catalysts, these complexes are easily isolated from the reaction suspension by a simple filtration and can be recycled with no less activity. The stability of the catalyst was confirmed by the powder X-ray diffraction (PXRD) pattern of **3a** and **2b** after the reactions (Figure S6 and S7, Supporting Information).

■ CONCLUSIONS

Two series of LnOFs based on the BTATB ligand were successfully designed and synthesized simply by using different solvents. Series A and B exhibit a novel 2D interdigitated (6,3) layer architecture and a 2D bilayer supermolecular structure, respectively. Their interesting structural features, lanthanide metal centers, and functional BTATB ligand impart these materials with excellent properties. **3a** exhibits strong luminescence emission in the solid state and in a methanol suspension at room temperature. **2b** exhibits near-infrared luminescence at 983 nm. More interesting is that the luminescence of **3a** displayed high selectivity for Zn^{2+}, which suggests that it may be used as a luminescent probe for Zn^{2+}. The amide groups on the BTATB ligand in the structures of **3a** and **2b** were used as a catalyst for the selective catalysis of organic molecules in the Knoevenagel condensation reaction. These results will facilitate the explora-

Table 3. Knoevenagel Condensation Reaction of Malononitrile and Ethyl Cyanoacetate with Substrates Catalyzed by 3a and 2b

run	substrate	molecular size	substrate	molecular size	catalyst	conversion
1					**3a**	99%
2		0.87nm / 0.61nm	0.69nm / 0.45nm		**2b**	33%
3				1.03nm / 0.45nm	**3a**	42%
4					**2b**	3%

tion of newly functionalized materials through the accessibility of functional organic linkers and metal components.

ASSOCIATED CONTENT

Ⓢ Supporting Information

Simulated and experimental X-ray powder diffraction patterns for series A and B; TGA curve of series A and B; excitation and emission spectra of **3a** in the solid state at room temperature; PXRD patterns of simulated and as-synthesized **3a** and **2b**; GC of the reactions of benzaldehyde and malononitrile and benzaldehyde and ethyl cyanoacetate catalyzed by **3a**; and GC of the reactions of benzaldehyde and malononitrile catalyzed by **2b**. This material is available free of charge via the Internet at http://pubs.acs.org.

AUTHOR INFORMATION

Corresponding Author

*E-mail: ceshzb@lnu.edu.cn.

Notes

The authors declare no competing financial interest.

ACKNOWLEDGMENTS

REFERENCES

(1) (a) Yaghi, O. M.; O'Keeffe, M.; Ockwig, N. W.; Chae, H. K.; Eddaoudi, M.; Kim, J. *Nature* **2003**, *423*, 705. (b) Zhang, J.-P.; Zhang, Y.-B.; Lin, J.-B.; Chen, X.-M. *Chem. Rev.* **2012**, *112*, 1001. (c) Li, J.-R.; Kuppler, R. J.; Zhou, H.-C. *Chem. Soc. Rev.* **2009**, *38*, 1477. (d) Ma, L.; Abney, C.; Lin, W. *Chem. Soc. Rev.* **2009**, *38*, 1248. (e) Cui, Y.; Yue, Y.; Qian, G.; Chen, B. *Chem. Rev.* **2012**, *112*, 1126. (f) Zeng, M.-H.; Wang, Q.-X.; Tan, Y.-X.; Hu, S.; Zhao, H.-X.; Long, L.-S.; Kurmoo, M. *J. Am. Chem. Soc.* **2010**, *132*, 2561.

(2) (a) Eliseeva, S. V.; Bünzli, J. C. G. *Chem. Soc. Rev.* **2010**, *39*, 189. (b) Armelaoa, L.; Quici, S.; Barigelletti, F.; Accorsic, G.; Bottaro, G.; Cavazzini, M.; Tondello, E. *Coord. Chem. Rev.* **2010**, *254*, 487.

(3) (a) Ma, L.; Evans, O. R.; Foxman, B. M.; Lin, W. B. *Inorg. Chem.* **1999**, *38*, 5837. (b) Richardson, F. S. *Chem. Rev.* **1982**, *82*, 541. (c) Parker, D.; Dickins, R. S.; Puschmamn, H.; Crossland, C.; Howard, J. A. K. *Chem. Rev.* **2002**, *102*, 1977. (d) Pandya, S.; Yu, J.; Parker, D. *Dalton Trans.* **2006**, 2757.

(4) Bünzli, J.-C. G.; Piguet, C. *Chem. Soc. Rev.* **2005**, *34*, 1048.

(5) (a) Rocha, J.; Carlos, L. D.; Paz, F. A. A.; Ananias, D. *Chem. Soc. Rev.* **2011**, *40*, 926. (b) Zhao, B.; Chen, X.-Y.; Cheng, P.; Liao, D.-Z.; Yan, S.-P.; Jiang, Z.-H. *J. Am. Chem. Soc.* **2004**, *126*, 15394. (c) Liu, W. S.; Jiao, T. Q.; Li, Y. Z.; Liu, Q. Z.; Tan, M. Y.; Wang, H.; Wang, L. F. *J. Am. Chem. Soc.* **2004**, *126*, 2280. (d) Chen, B. L.; Wang, L. B.; Xiao, Y. Q.; Fronczek,

F. R.; Xue, M.; Cui, Y. J.; Qian, G. D. *Angew. Chem., Int. Ed.* **2009**, *48*, 500. (e) Zheng, M.; Tan, H. Q.; Xie, Z. G.; Zhang, L. G.; Jing, X. B.; Sun, Z. C. *ACS Appl. Mater. Interfaces* **2013**, *5*, 1078. (f) Chen, Z.; Sun, Y.; Zhang, L.; Sun, D.; Liu, F.; Meng, Q.; Wang, R.; Sun, D. *Chem. Commun.* **2013**, *49*, 11557.

(6) (a) Burgoyne, A. R.; Meijboom, R. *Catal. Lett.* **2013**, *143*, 563. (b) Hwang, Y.; Hong, D.-Y.; Chang, J.-S.; Jhung, S. H.; Seo, Y.-K.; Kim, J.; Vimont, A.; Daturi, M.; Serre, C.; Férey, G. *Angew. Chem., Int. Ed.* **2008**, *47*, 4144.

(7) (a) Llabrés i Xamena, F. X.; Casanova, O.; Tailleur, R. G.; Garcia, H.; Corma, A. *J. Catal.* **2008**, *255*, 220. (b) Llabrés i Xamena, F. X.; Abad, A.; Corma, A.; Garcia, H. *J. Catal.* **2007**, *250*, 294.

(8) (a) Hasegawa, S.; Horike, S.; Matsuda, R.; Furukawa, S.; Mochizuki, K.; Kinoshita, Y.; Kitagawa, S. *J. Am. Chem. Soc.* **2007**, *129*, 2607. (b) Wang, Z. Q.; Cohen, S. M. *J. Am. Chem. Soc.* **2007**, *129*, 12368. (c) Millward, A. R.; Yaghi, O. M. *J. Am. Chem. Soc.* **2005**, *127*, 17998. (d) Seo, J. S.; Whang, D.; Lee, H.; Jun, S. I.; Oh, J.; Jeon, Y. J.; Kim, K. *Nature* **2000**, *404*, 982.

(9) (a) Zhang, J.; Wojtas, L.; Larsen, R. W.; Eddaoudi, M.; Zaworotko, M. J. *J. Am. Chem. Soc.* **2009**, *131*, 17040−17041. (b) Zhang, M.-Y.; Shan, W.-J.; Han, Z.-B. *CrystEngComm* **2012**, *14*, 1568. (c) Xiao, J.; Liu, B.-Y.; Wei, G.; Huang, X.-C. *Inorg. Chem.* **2011**, *50*, 11032.

(10) (a) Ghosha, S. K.; Kitagawa, S. *CrystEngComm* **2008**, *10*, 1739. (b) Cundy, C. Y.; Cox, P. A. *Microporous Mesoporous Mater.* **2005**, *82*, 1.

(11) *SHELXTL 6.10*; Bruker Analytical Instrumentation: Madison, WI, 2000.

(12) Lu, W.-J.; Zhang, L.-P.; Song, H.-B.; Wang, Q.-M.; Mak, T. C. W. *New J. Chem.* **2002**, *26*, 775.

(13) Wang, F.-Q.; Zheng, X.-J.; Wan, Y.-H.; Sun, C.-Y.; Wang, Z.-M.; Wang, K.-Z.; Jin, L.-P. *Inorg. Chem.* **2007**, *46*, 2956.

(14) He, Y.-K.; Han, Z.-B.; Ma, Y.; Zhang, X.-D. *Inorg. Chem. Commun.* **2007**, *10*, 829.

(15) (a) Batten, S. R.; Robson, R. *Angew. Chem., Int. Ed. Engl.* **1998**, *37*, 1460. (b) Bu, Y.; Jiang, F.; Zhou, K.; Li, X.; Zhang, L.; Gai, Y.; Hong, M. *CrystEngComm.* **2013**, *15*, 8426.

(16) (a) Subhash, C. G.; Michael, A. M.; Michael, Y. C.; William, E. B. *J. Am. Chem. Soc.* **1991**, *113*, 1844. (b) Annika, M. P.; Westin, L. G.; Mikael, K. *Chem.—Eur. J.* **2001**, *7*, 3439. (c) Thomas, D.; Michel, E.; Yves, M. L.; Enric, C.; Pascale, A.-S.; Marc, F.; Patrick, B. *J. Am. Chem. Soc.* **2003**, *125*, 3295.

(17) Zheng, S.-R.; Yang, Q.-Y.; Liu, Y.-R.; Zhang, J.-Y.; Tong, Y.-X.; Zhao, C.-Y.; Su, C.-Y. *Chem. Commun.* **2008**, 356.

(18) Hill, R. J.; Long, D.-L.; Turvey, M. S.; Blake, A. J.; Champness, N. R.; Hubberstey, P.; Wilson, C.; Schröder, M. *Chem. Commun.* **2004**, 1792.

(19) Wang, J.-J.; Gou, L.; Hu, H.-M.; Han, Z.-X.; Li, D.-S.; Xue, G.-L.; Yang, M.-L.; Shi, Q.-Z. *Cryst. Growth Des.* **2007**, *7*, 1514.

(20) (a) Arnaud, N.; Vaquer, E.; Georges, J. *Analyst* **1998**, *123*, 261. (b) Reineke, T. M.; Eddaoudi, M.; Fehr, M.; Kelley, D.; Yaghi, O. M. *J. Am. Chem. Soc.* **1999**, *121*, 1651.

(21) (a) Bo, Q.-B.; Sun, G.-X.; Geng, D.-L. *Inorg. Chem.* **2010**, *49*, 561. (b) Guo, X.; Zhu, G.; Fang, Q.; Xue, M.; Tian, G.; Sun, J.; Li, X.; Qiu, S. *Inorg. Chem.* **2005**, *44*, 3850. (c) Jin, J.; Niu, S.; Han, Q.; Chi, Y. *New J. Chem.* **2010**, *34*, 1176. (d) Wang, H.-S.; Zhao, B.; Zhai, B.; Shi, W.; Cheng, P.; Liao, D.-Z.; Yan, S.-P. *Cryst. Growth Des.* **2007**, *7*, 1851.

3008

dx.doi.org/10.1021/cg500286v | *Cryst. Growth Des.* 2014, 14, 3002−3009

(e) Quici, S.; Cavazzini, M.; Marzanni, G.; Accorsi, G.; Armaroli, N.; Ventura, B.; Barigelletti, F. *Inorg. Chem.* **2005**, *44*, 529.

(22) (a) An, J.; Shade, C. M.; Chengelis-Czegan, D. A.; Petoud, S.; Rosi, N. L. *J. Am. Chem. Soc.* **2011**, *133*, 1220. (b) Imbert, D.; Cantuel, M.; Bünzli, J.-C. G.; Bernardinelli, G.; Piguet, C. *J. Am. Chem. Soc.* **2003**, *125*, 15698. (c) Zhang, J.; Badger, P. D.; Geib, S. J.; Petoud, S. *Angew. Chem., Int. Ed.* **2005**, *44*, 2508. (d) White, K. A.; Chengelis, D. A.; Gogick, K. A.; Stehman, J.; Rosi, N. L.; Petoud, S. *J. Am. Chem. Soc.* **2009**, *131*, 18069.

(23) (a) Fang, Q.-R.; Yuan, D.-Q.; Sculley, J.; Li, J.-R.; Han, Z.-B.; Zhou, H.-C. *Inorg. Chem.* **2010**, *49*, 11637. (b) Gascon, J.; Aktay, U.; Hernandez-Alonso, M. D.; van Klink, G. P. M.; Kapteijn, F. *J. Catal.* **2009**, *261*, 75. (c) Canivet, J.; Aguado, S.; Schuurman, Y.; Farrusseng, D. *J. Am. Chem. Soc.* **2013**, *135*, 4195.